Energy Technology
Generation, Conversion, Storage, Distribution
www.entechnol.de

Properties and Structural Arrangements of the Electrode Material CuDEPP during Energy Storage

*Christoph Karsten Jung, Daniel Stottmeister, and Timo Jacob**

Devices for electrical energy storage need to provide high energy yields and output power, guaranteeing at the same time safety, low costs, and long operation times. The porphyrin CuDEPP [5,15-bis(ethynyl)-10,20-diphenylporphinato] copper(II) is a promising electrode material for various battery systems both as anode and cathode. While its functionality has been demonstrated experimentally, there is no atomistic information as to why CuDEPP expresses these interesting properties or how the incorporation of ions affects its structure so far. To answer these questions, CuDEPP is investigated using density functional theory (DFT). Starting with the smallest possible unit (i.e., a single molecule), the spatial dimensionality of the structure is successively increased by studying: 1) di- and trimers, 2) molecular stacking in a 1D chain, 3) extending these chains to planar CuDEPP sheets, and finally 4) a three-dimensionally extended polymer structure. Having thoroughly investigated the isolated properties of the CuDEPP material itself, afterward the insertion (or intercalation) of different ions (including Li, Mg, and Na) is studied, to understand the energetics, diffusion barriers, and structural changes (e.g., volume expansion) within the CuDEPP host material.

1. Introduction

In recent years, the demand for electrical energy storage solutions has risen, being pushed, for instance, by global environmental issues.[1,2] Devices for this purpose need to provide both high energy yield and high output power, guaranteeing at the same time safety, low costs, and long life.[3,4]

Furthermore, aiming for more sustainable energy storage systems research needs to shift from using nonrenewable resources to more earth-abundant materials. Here, organic electrodes, showing low life-cycle costs and lower waste production, seem to be possible and promising candidates. Nevertheless, low electrical conductivity and dissolution in the electrolyte are still problems being faced by organic electrodes.[4,5]

Porphyrin CuDEPP [5,15-bis(ethynyl)-10,20-diphenylporphinato] copper(II) is a metalloporphyrin having multielectron redox activities and is a promising organic electrode material for various battery technologies, featuring the ability of acting as an electron donor or acceptor.[6–10] In contrast to the slow discharge/charge processes in traditional lithium-ion batteries, the CuDEPP electrode features a fast redox conversion in which up to four electrons are transferred.[9] CuDEPP combines the positive properties of lithium-ion batteries (high energy density[9]) with those of a supercapacitor (quick electron release and absorption).[11] Interestingly, natural substances such as chlorophyll, heme (in hemoglobin), and cobalamin (vitamin B12) show a similar structure.[11–13]

The multifunctional electrode material CuDEPP—its functionality has already been demonstrated experimentally—opens up new ways for the design of organic electrode materials due to its excellent properties.[6,9,11–13] However, up to now there is no atomistic information as to why CuDEPP expresses these qualities or how the incorporation of lithium affects its structure and stability. To answer these questions, in the current work we have investigated CuDEPP using density functional theory (DFT). We studied the behavior of an extended set of possible structural organizations and conformations of the CuDEPP molecular arrangement with an increasing level of dimensionality. Starting with single molecular units and dimers (0D), the complexity was increased by considering chains (1D, staircase shape), sheets (2D, extended staircase shape), and even bulk structures (3D, layered staircase shape). After determining the structural network, the impact of charge storage and release was considered by studying the energetics of ion insertion/intercalation. Finally, the pronounced role of the central Cu atom in the CuDEPP structures is elucidated with respect to the energetics and the calculated voltage curves for lithium intercalation.

C. K. Jung, D. Stottmeister, Prof. T. Jacob
Institute of Electrochemistry
Ulm University
Albert-Einstein-Allee 47, 89081 Ulm, Germany
E-mail: timo.jacob@uni-ulm.de

C. K. Jung, Prof. T. Jacob
Helmholtz-Institute Ulm (HIU) for Electrochemical Energy Storage
Helmholtzstr. 11, 89081 Ulm, Germany

C. K. Jung, Prof. T. Jacob
Karlsruhe Institute of Technology (KIT)
P.O. Box 3640, 76021 Karlsruhe, Germany

The ORCID identification number(s) for the author(s) of this article can be found under https://doi.org/10.1002/ente.202000388.

DOI: 10.1002/ente.202000388

2. Results and Discussion

2.1. Single CuDEPP Molecule

The energetically most stable structure of a single CuDEPP molecule is shown in **Figure 1**. The bond length of the ethynyl group is 1.22 Å (between C25 and C24 carbons, or respectively C27 and C26) and thus corresponds to a triple bond. The energetically preferred angle between the phenyl ring and the plane spanned by the four nitrogen atoms is 109.6° on the exchange correlation functional by Perdew–Burke–Ernzerhof (PBE) level, whereas the PBE0 hybrid functional leads to a slightly smaller angle of 108.8°. The rotational barrier is below 0.1 eV for angular distortions of ±20° (see Supporting Information). These results (obtained with the molecular DFT-program Jaguar) were then compared with a periodic plane-wave treatment (based on Vienna Ab initio Simulation Package [VASP]), as all further systems were studied with the latter one due to their periodic nature. Both DFT treatments showed very similar behaviors for structural and energetic features of the single CuDEPP molecule. Both the periodic and the cluster calculations optimized the electronic structure to a doublet state. All measured bond lengths are showing only minor deviations of a maximum of 0.1 Å between the two DFT approaches. Selected bond lengths can be found in **Table 1**. The charge distribution shows the same trends for both the cluster and the plane-wave code. While (as expected) the exact charge distributions do not match due to differences in the two techniques, the general charge donation/acception trends coincide. In fact Cu turns out to be partially positively charged by 0.5 e^- and the nitrogen atoms are partially negatively charged (–0.1 e^-). Moreover, the carbon atoms in the porphyrin ring carry equal charges (–0.05 to –0.2 e^-), suggesting a delocalization of the electrons. The bonds C26—C27 and C24—C25 show a higher charge agglomeration, fitting well the hypothesis of a triple bond at this position. All charge distributions can be found in the Supporting Information.

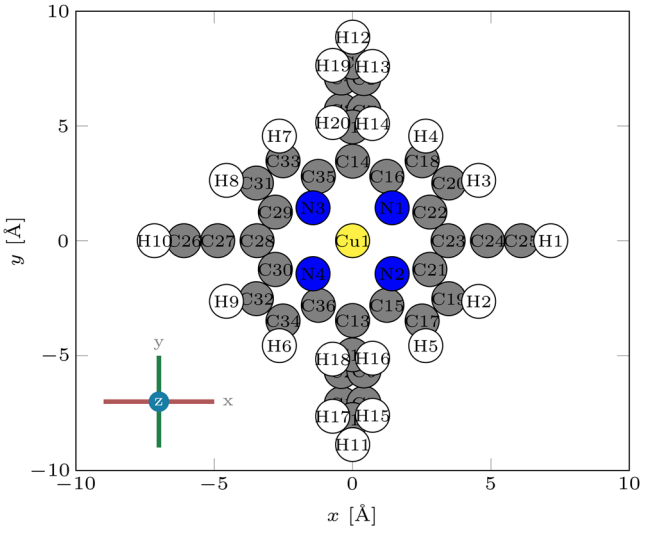

Figure 1. Energetically preferred CuDEPP structure.

Table 1. Comparison of selected bond lengths. All values are given in Å.

Bond	VASP (PBE)	Jaguar (PBE, PBE0)
C18—C20	1.37	1.36
C18—C16	1.45	1.44
N1—Cu1	2.03	2.02

2.2. Stacked CuDEPP Structures

The crystal structure of CuDEPP has previously been determined by powder X-ray diffraction, suggesting a stacking of the molecules (similar to a molecular staircase),[14] as being indicated in **Figure 2**. While the steric demand of the phenyl groups is limiting the number of configurations to only a few possible (and feasible) arrangements, the stabilization of the ethynyl group is playing a dominant role. Due to the periodic nature of this molecular staircase, all the forthcoming calculations were performed with the VASP program suite (for details, see above). Our studies reveal that Cu is interacting with the ethynyl group of the molecules above and below, as shown in Figure 2. Modifying the intermolecular distance d_z step-wise, an optimal distance in the range between 3.1 and 3.3 Å was found, being in good agreement with the corresponding XRD data ($d_{exp} = 3.24$ Å). In this distance range around the minimum (3.1–3.3 Å), the interaction energy varies by only maximum 0.01 eV, being indicative of weak interactions between the staircase-like arranged CuDEPP molecules, which we calculated to be –0.4 eV per molecule. It should be emphasized that in this arrangement the ethynyl groups bend from the plane toward the Cu. Here, the height difference in z-direction is 1.2 Å between H1 and H10, as can be seen in Figure 2.

To estimate the steric deformation caused by the stacking, in a corresponding calculation we removed the molecules above and below the central CuDEPP molecule and (while keeping the structure of the central molecule fixed) recalculated the stability of the molecule in this curved shape. Here, we find that the morphological distortion caused by the neighboring molecules changes the energy negligibly by <0.001 eV. As a consequence

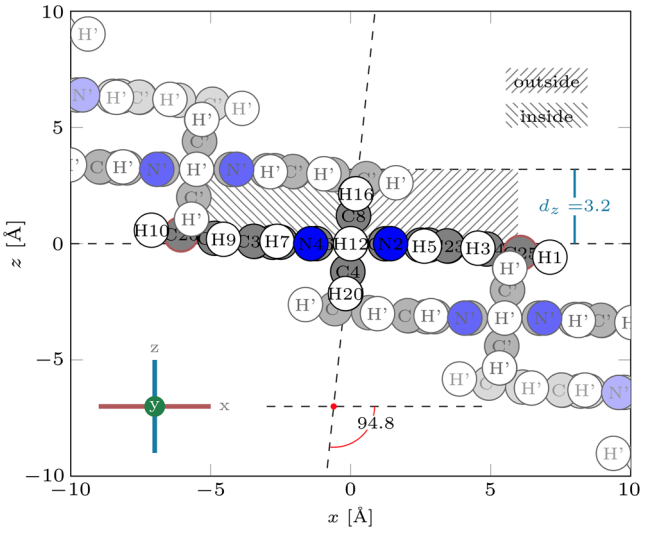

Figure 2. Schematic representation of the stacked CuDEPP structure. Note the different hatching orientations for the inside and outside parts.

of the weak molecular interactions, no changes in the bond lengths between the 0D (sole CuDEPP molecule) and the 1D staircase structure could be observed. However, the preferred angle between the nitrogen plane and the phenyl groups changes from 109.6° to 94.8°, as shown in Figure 2.

2.3. Extended Staircase CuDEPP Structures

While in the previous section we have studied the 1D staircase-shaped CuDEPP structures units along the *z*-axis, we now concentrate on 2D-extended structures resulting from molecular arrangements along the *y*–*z* plane. A table summarizing the corresponding energies and distances can be found in the Supporting Information.

In the most stable extended staircase configuration (see **Figure 3**), the molecules are shifted in the plane to each other. Therefore, hereafter this configuration is called *shifted extended staircase*. In this structure the interaction energy between the molecules is –1.1 eV (around –0.5 eV per phenyl group pair). As shown in Figure 3a, the phenyl groups are overlapping along the *x*- and *z*-directions of the periodic repetitions. The optimal intermolecular distance (layering distance) d_z remains at 3.2 Å.

In this extended staircase, there is no interaction in the *x*-direction. The optimization of this third spatial direction (axis along H1 and H10) leads to a quite different structure.

From a bonding point of view, polymerization takes place via the ethynyl group, and the formation of a covalent sigma bond between the molecules (and two double bonds) occurs. The sigma bond is formed between C25 and C26 in the periodically continued (*x*-direction) CuDEPP structure. The polymerization of CuDEPP has been proven experimentally by analyzing the characteristic ethynyl stretching vibrational modes.[9]

Layering of the extended staircase (leading to a *bulk structure*) without forming a covalent bond (H1 and H10′ are close) causes minor changes in the energetics.

2.4. Polymeric CuDEPP Structures

As it was done for the noncovalently bound molecules, we have investigated the possible periodic arrangement of the covalently bound polymeric CuDEPP structure. Here, the structure shown in **Figure 4** is particularly interesting. We call this structure *sheet polymer* (stacking of the covalent bonded molecules, no interaction between these sheets). If one considers the nitrogens of each CuDEPP molecule as a plane, the planes of the unit lying above and below are tilted. The phenyl groups are rotated in an alternating fashion and exhibit a sharp angle to each other. Ab initio molecular dynamic (MD) simulations containing one or more Li reveal that the ethynyl groups close up around these Li atoms. The height difference between H1 and H10 increases to a distance of up to 4 Å. This suggests the polymerization being a consequence of this rearrangement. Nevertheless, further studies on the exact polymerization process would be required.

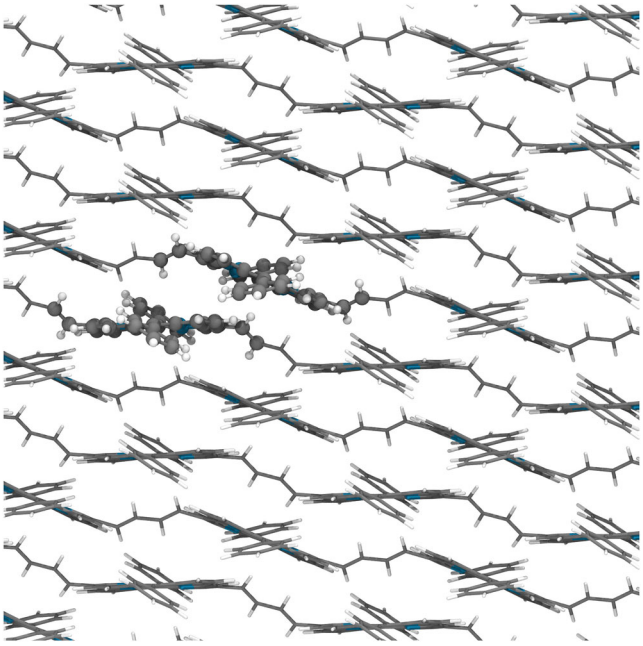

Figure 4. Schematic representation of the periodically continued covalently bound sheet polymer structure. Van der Waals representation of the atoms belonging to the central unit cell.

Solely based on DFT, our extensive search for possible arrangements of a 3D-ordered structure was not successful. Either there are structures with attractive interactions along

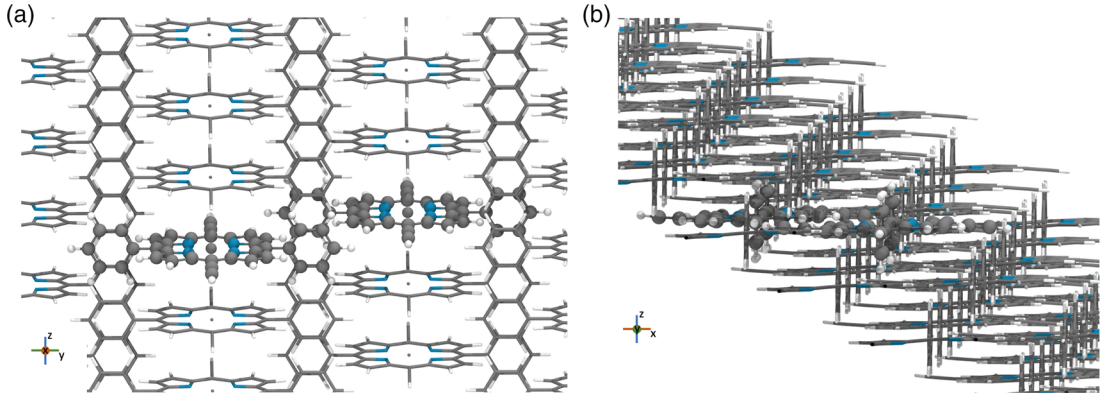

Figure 3. Representation of the extended staircase shaped CuDEPP structure in two different views. Atoms belonging to the central unit cell are shown in a van der Waals representation: a) view direction *x*–*z*; b) view direction *y*–*z*.

the *y*- and *z*-directions (see single molecules) or along the *z*- and *x*-directions, but never along all three directions. Therefore, we performed ReaxFF reactive force field simulations that allowed investigations of larger systems as well as more extensive explorations of the configurational space.[15,16] Based on these screening studies we found that a twisted arrangement of the molecules is likely to have the overall lowest energy (see Supporting Information). Interestingly, in this type of arrangement the phenyl groups are able to interact again.

Regarding the electronic structure we find that the gap between the highest-occupied-molecular-orbital (HOMO) and the lowest-unoccupied-molecular-orbital (LUMO) is reduced due to polymerization.[6] For instance, the bandgap for the molecular staircase CuDEPP arrangement is 1.3 eV, whereas for the extended staircase and the bulk arrangement the bandgap decreases to 1.0 eV. For the sheet polymeric (covalent bond) system shown in Figure 4, the bandgap becomes 0.4 eV. Of course, it is well known that bandgaps evaluated on the DFT level are usually underestimated, that is why the exact values should be taken with caution. However, the behavior shows the general trend that the bandgap reduces with increasing dimensionality. As a consequence, we expect an enhanced electron transfer for more complex structures and therefore an increased electronic conductivity with increasing dimensionality. This behavior was already observed by electrochemical impedance spectroscopy.[6]

2.5. Insertion Processes of Li

In battery materials/electrodes, charging and discharging processes involve the insertion of ions inside a structure. Therefore, we investigated the incorporation of Li into the extended staircase, the bulk and the sheet polymeric CuDEPP structures. At first, one Li was placed at five different positions (e.g., top (pos. 1), bridge inside/outside (pos. 2, 3), N–N inside/outside (pos. 4, 5)) as shown in **Figure 5**. The difference between inside and outside is shown in Figure 2 and 5. **Table 2** shows the intercalation energies and optimal d_z for lithium at the different respective positions. A single lithium atom energetically prefers the bridge outside position (pos. 3). Apart from the top position (pos. 1), the energy at all other positions is within a difference of only 0.2 eV. The energetically preferred distance d_z changes only slightly (under 0.1 Å), at least in the cases of the positions pos. 2, pos. 3, and pos. 5. Filling only the top position (pos. 1) would lead to a volume increase of around 16%. To provide a first estimate of the diffusion barriers, we then performed a series of ab initio MDs simulations at 300 K. Positions pos. 2 to pos. 5 were taken as the starting point for the ab initio MDs simulations and a barrier was then estimated from the energy course of all MDs. Given the fact that the intercalation energy is rather similar at all considered sites, during the MD simulations, we indeed could observe migration of the Li atoms along all considered sites. From these studies we estimated the energy barrier for diffusion to be around 0.5 eV. Of course, more detailed transition state search studies are necessary to obtain the exact diffusion barriers, but this was out of the scope of the current work.

Afterward, we successively increased the number of intercalated Li up to six atoms per CuDEPP molecule. The resulting voltage curves for increasing numbers of Li in the three different structures are shown in **Figure 6**. The reference for the voltage curve is bulk Li.

Table 2. Intercalation energies and optimal distances d_z for lithium.

Position	E_{Li} [eV]	d_z [Å]
Top (1)	−2.54	3.7
Bridge inside (2)	−2.98	3.1
Bridge outside (3)	−3.04	3.2
N–N inside (4)	−2.82	3.4
N–N outside (5)	−2.97	3.1

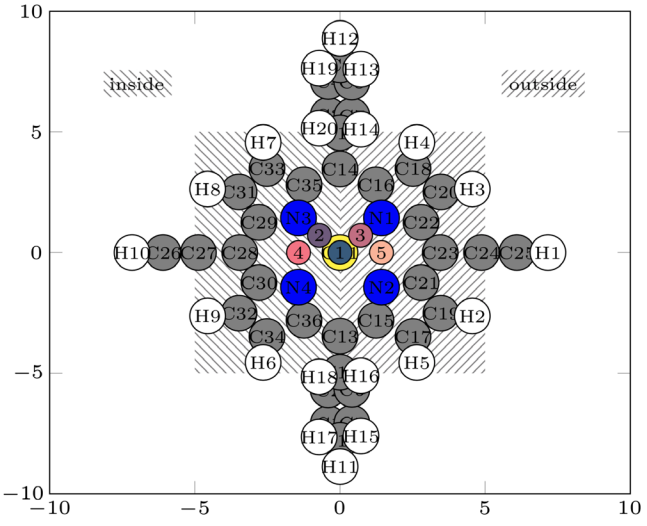

Figure 5. Five positions of the intercalated ions (numbered and named pos. 1 to pos. 5 near the center of the structure). Energies and distances d_z can be found in Table 4. Distances at the axes are in Å. See Figure 2 for additional inside and outside definition (different hatching direction).

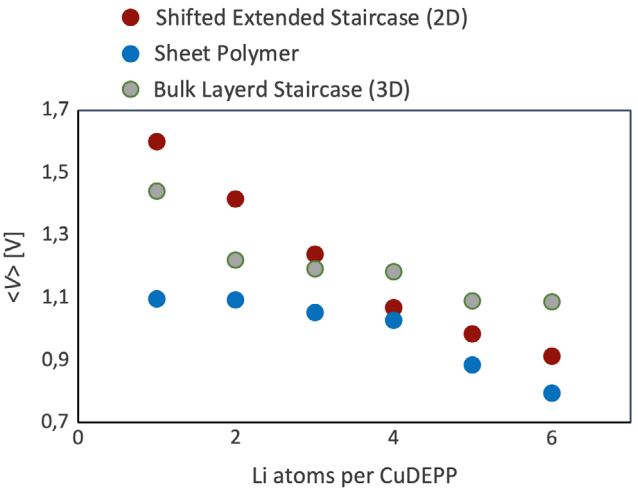

Figure 6. Voltage for the step-by-step intercalation of Li into the configurations: shifted extended staircase, the 3D bulk, and the sheet polymeric CuDEPP structure.

One can see that the behavior for the extended staircase and for the bulk structures is rather similar: starting at around 1.5 V the average voltage decreases with every added Li. In the case of the polymer, the decrease has a lower slope. Overall, the voltage of the sheet polymer is smaller. In summary, Figure 6 shows that lithium is bound weaker in the polymer structure than in the noncovalently bound ones. These results characterize our three different structures. However, they do not give any indication of mechanisms nor do six Li per CuDEPP correspond to a full load.

This can be seen in particular in the energy density, as shown in Table S10, Supporting Information. Table S10, Supporting Information, contains the theoretical energy densities for the storage of one to six lithium per CuDepp molecule for the respective structures dictated here. The maximum theoretical energy density resulting from this table is still 50 Wh kg^{-1} lower than the energy density Gao et al. presented.[9]

Structurally, there is a difference between noncovalent and covalent molecules: Li displaces (0.1–0.2 Å displacement of the Cu) the Cu atom in the center of extended staircase and for the bulk structures, with the ethynylene group of the underlying CuDEPP layer carrying the now-exposed Cu center. In the sheet polymer, this Cu pushing out is not observed.

Atom-projected density of states (DoS) for the increasing Li content can be found in the Supporting Information. As stated before, the empty system is in a doublet state. Incorporation of Li changes the overall state to a singlet and causes a rising Fermi level (see Supporting Information). From one to four incorporated Li one can see changes in the p-band of the carbon atoms. Five and six Li affect the d-band of the central Cu (DoS shifted slightly to lower energies). These results can also be expected from the charge distribution. To better understand the incorporation of Li into the CuDEPP structure as well as the induced electronic effects, we afterward analyzed the charge density distribution before and after incorporation (see Supporting Information). **Figure 7** shows the charge density of the extended staircase CuDEPP structure. As can be seen, charge is transferred from the conjugated ring to the Li atoms. Mulliken analysis shows a +0.2 e^- net charge on all Li (top two in the figure). The Li in the N–N inside (pos. 4) has a net charge of +0.1 e^-.

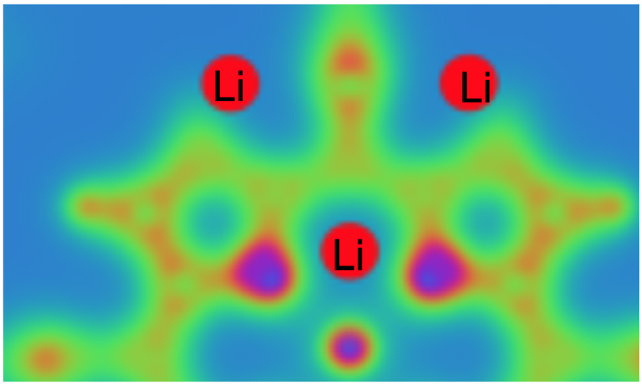

Figure 7. Charge density distribution along the central molecular plane of CuDEPP after insertion of three Li atoms (marked in red). These Li are sitting above the cutting plane. Near the Li one can see a lower charge density in the CuDEPP plane.

So far, the obtained results are in very good agreement with the experimental data: First, with an increasing degree of polymerization, the electronic conductivity increases. Second, the voltage for Li insertion decreases when moving from a single CuDEPP molecule to the full polymer. Furthermore, the function of Cu as the central atom becomes clear. This structural rearrangement by pushing the Cu out of its position seems to stabilize the incorporation of Li, at least in the noncovalently bounded structures. Nevertheless, further studies of the detailed incorporation need to be performed.

2.6. Insertion Processes of Alternative Ions

To explore the potential of this material, apart from Li, relevant alternative ions (i.e., cations: Na^+, Mg^{2+}; anions: PF_6^-, BF_4^-, ClO_4^-) were placed between the molecules. For sodium insertion, the N–N outer position was found to be the most stable one, whereas the N–N inside position is nearly degenerate. The other possible intercalation spots are less favorable by 0.5–0.8 eV. The insertion energy of Mg is at least 0.8 eV lower compared with Li and it is remarkable that Mg replaces Cu as the central atom (see **Figure 8**).

The formation energy in **Table 3** confirms this observation because magnesium forms a strong bond with the nitrogen ring.

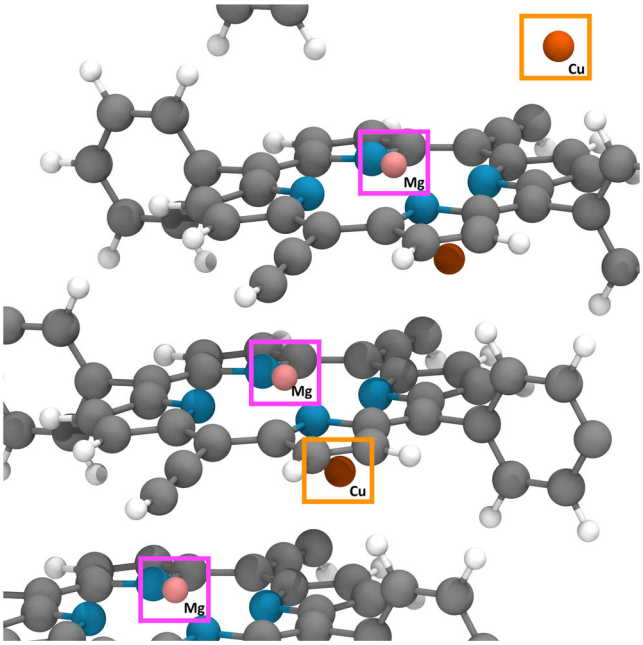

Figure 8. Structure of Mg (shown here in pink) intercalation in CuDEPP, showing the displacement of Cu (in orange) as the central atom.

Table 3. Comparison of selected bond lengths. All values are given in Å.

System	E_{int} [eV]	Spring constant
CuDEPP	−8.32	2.72
MgDEPP	−9.27	1.74

Table 4. Intercalation energies and optimal distances d_z for sodium and magnesium.

Position	E_{Na} [eV]	d_{Na} [Å]	E_{Mg} [eV]	d_{Mg} [Å]
Top (1)	−2.31	3.6	−3.9	3.5
Bridge inside (2)	−2.14	3.1	−3.8	3.7
Bridge outside (3)	−3.14	3.5	−3.8	3.6
N–N inside (4)	−2.84	3.4	−3.8	3.6
N–N outside (5)	−2.98	3.0	–	–

Table 5. Intercalation energies and optimal distance d_z for different intercalating ions.

intercalating ions	E_{int} [eV]	d_z [Å]	ΔE_{diff}
Na	−2.98	3.0	0.37
Mg	−3.90	3.5	
2 × Mg	−1.89	3.7	
3 × Mg	−2.13	3.7	
PF_6	−2.61	7.1	0.86
2 × PF_6	−2.82	5.9	
3 × PF_6	−2.79	5.9	
BF_4	−2.35	5.4	
2 × BF_4	−2.84	5.0	
3 × BF_4	−2.59	5.6	
ClO_4	−0.93	5.4	
2 × ClO_4	−1.27	5.2	
3 × ClO_4	−1.30	5.8	

Based on our data, MgDEPP (Mg as central atom) should be an ideal alternative candidate for Cu replacement.

Furthermore, the optimal layer spacing of sodium is not much larger (approximately 0.1 Å) than in the Li–CuDEPP system. The preferred positions are the same for Li and Na. As shown in **Table 4**, sodium is more strongly bound between the layers. With Na bulk as reference, the intercalation energy of one sodium is −1.69 eV and thus higher than the intercalation energy of Li (−1.49 eV with bulk Li as reference). This system would result in a slight voltage increase compared with the Li–CuDEPP system.

In the following, the insertion of multiple ions has been investigated and the corresponding results are shown in **Table 5**. The intercalation of the anions PF_6, BF_4, and ClO_4 revealed considerably larger CuDEPP–CuDEPP distances, which is attributable to their sizes. In particular, PF_6 is remarkable as it leads to an increased distance between the CuDEPP layers of 7.1 Å. An insertion of these larger anions is thus associated with an increase in volume of up to 50%.

3. Conclusions

In this study, atomistic simulations of CuDEPP allowed us not just to shed light on the unique properties of this material but also to elucidate the effect of ionic intercalation. Starting with the smallest possible unit (i.e., a single molecule), we successively increased the spatial dimensionality of the structure. We have shown a structure where the interactions of the molecules are most stable from an energetic point of view. The overlapping of the phenyl groups and the interaction of the ethylene group and the Cu central atom contribute mainly to the stabilization. The 3D extended polymer structure is energetically favored, which matches the experimental observations. After having thoroughly investigated the properties of the isolated CuDEPP, the insertion (or intercalation) of different ions (including Li, Mg, and Na) has been studied to understand the energetics, diffusion barriers, and structural changes (e.g., volume expansion) within the CuDEPP host material. Based on the optimal ion intercalation structure, discharge voltage curves have been calculated. The thus-obtained cell voltages can be directly compared with experimental measurements. Magnesium can be pointed out as possible candidate for an alternative central atom (instead of Cu). This MgDEPP structure together with sodium as intercalation ion could indeed be a promising candidate for a post lithium battery system.

4. Experimental Section

Periodic DFT calculations were performed using the VASP [17,18] with a cutoff energy of 400 eV. Structures were optimized geometrically up to a convergence criterion of 0.0001 eV and all forces below 0.001 eV $Å^{-1}$. The exchange correlation was calculated using the PBE functional of Perdew, Burke, and Ernzerhof within the generalized–gradient–approximation (GGA).[19,20] A converged ***k***-point sampling with a density of 0.18 $Å^{-1}$ was used. Dispersion interactions were treated on the DFT-D3 level.[21,22] For sake of consistency, the bulk lithium and sodium calculations were also performed with the D3 correction. It is always indicated where bulk reference was used. For all other cases, one atom or molecule was used in a sufficiently large simulation box. Cell voltages were calculated applying the scheme suggested by Cococcioni et al.[23–26] The average voltage $\langle V \rangle$ is calculated as

$$\langle V \rangle = -\frac{G(\mathrm{Li}_{\Delta x}\mathrm{CuDEPP}) - G(\mathrm{Li}_0\mathrm{CuDEPP}) - \Delta x G(\mathrm{Li})}{e \cdot \Delta x} \quad (1)$$

where G is the Gibbs free energy. Neglecting pressure and entropy contributions, which are small or mainly cancel out, the Gibbs free energy can be replaced with the ground state energies.

Equation (1) implies the following insertion reaction

$$\Delta x\,\mathrm{Li} + \mathrm{CuDEPP} \Leftrightarrow \mathrm{Li}_{\Delta x}\mathrm{CuDEPP} \quad (2)$$

Partial (***k***-point decomposed) charge density distributions were evaluated utilizing VASP and visualized in visual MDs;[27] Bader,[28] Mulliken,[29] and Löwdin[30] charge analyses were performed for partial atomic charge evaluations. The latter two were performed within the LOBSTER framework.[31,32]

While periodic systems were treated as described earlier, molecular systems were additionally studied using the Jaguar program suite.[33] These calculations were performed at the PBE/LACV3P^{++} as well as PBE0/LACV3P^{++} level. For atomic partial charges, Mulliken[29] and Löwdin[30] population analyses were performed.

Ab initio MDs (as implemented in VASP[17,18]) were typically run for 4 ps within the microcanonical ensemble by solving the classical equation of motions with the help of the Verlet algorithm and a time step of 0.5 fs.

For the more extended systems, reactive force field simulations were performed using ReaxFF.[15,34] Here, after extensive tests the reactive force field[15] of Xiao Hu, Jörg Schuster, and Stefan E. Schulz was applied to

study the CuDEPP systems.[16] All ReaxFF simulations were carried out using the Amsterdam Modeling Suite 2018.[35]

The influence of individual structural changes such as the rotation of a monomer unit or the distance between two polymer strands was screened separately via single-point energy determination (about 10^7 structures). The most stable structures resulting from this sampling were then used in subsequent DFT calculations for a detailed evaluation of morphology and electronic structure.

Supporting Information

Supporting Information is available from the Wiley Online Library or from the author.

Acknowledgements

This work was supported by the German Research Fojndation (DFG) under project ID 390874152 (POLiS Cluster of Excellence) as well through the SPP-2248 (Polymer-based Batteries). Furthermore, computational resources were provided by the state of Baden-Württemberg through bwHPC and the German Science Foundation (DFG) under grant no. INST 40/467-1 FUGG.

Conflict of Interest

The authors declare no conflict of interest.

Keywords

batteries, computational chemistry, electrode materials, polymers, sustainable chemistry

Received: April 27, 2020
Revised: June 8, 2020
Published online:

[1] M. S. Guney, Y. Tepe, *Renew. Sustain. Energy Rev.* **2017**, *75*, 1187.
[2] C. Zhang, Y. L. Wei, P. F. Cao, M. C. Lin, *Renew. Sustain. Energy Rev.* **2018**, *82*, 3091.
[3] J. B. Goodenough, K. S. Park, *J. Am. Chem. Soc.* **2013**, *135*, 1167.
[4] J. M. Tarascon, M. Armand, *Nature* **2001**, *414*, 359.
[5] K. Pirnat, G. Mali, M. Gaberscek, R. Dominko, *J. Power Sources* **2016**, *315*, 169.
[6] Z. Zhao-Karger, P. Gao, T. Ebert, S. Klyatskaya, Z. Chen, M. Ruben, M. Fichtner, *Adv. Mater.* **2019**, 31.
[7] A. Antoniuk-Pablant, Y. Terazono, B. J. Brennan, B. D. Sherman, J. D. Megiatto Jr, G. W. Brudvig, A. L. Moore, T. A. Moore, D. Gust, *J. Mater. Chem. A.* **2016**, *4*, 2976.
[8] Z. Chen, P. Gao, W. Wang, S. Klyatskaya, Z. Zhao-Karger, D. Wang, C. Kübel, O. Fuhr, M. Fichtner, M. Ruben, *ChemSusChem.* **2019**, *12*, 3737.
[9] P. Gao, Z. Chen, Z. Zhao-Karger, J. E. Mueller, C. Jung, S. Klyatskaya, T. Diemant, O. Fuhr, T. Jacob, R. J. Behm, M. Ruben, M. Fichtner, *Angew. Chem. Int. Ed.* **2017**, 56.
[10] M. K. Chahal, M. Sankar *RSC Adv.* **2015**, *5*, 99028.
[11] B. Feng, J. Zhang, Q. Zhong, W. Li, S. Li, H. Li, P. Cheng, S. Meng, L. Chen, K. Wu, *Nat. Chem.* **2016**, *8*, 563.
[12] I. Fleming, *Nature* **1967**, *216*, 151.
[13] A. Eschenmoser, *Angew. Chem. Int. Ed.* **1988**, *27*, 5.
[14] M. Yao, H. Senoh, S. I. Yamazaki, Z. Siroma, T. Sakai, K. Yasuda, *J. Power Sources* **2010**, *195*, 8336.
[15] K. Chenoweth, A. C. T. Van Duin, W. A. Goddard, *J. Phys. Chem. A* **2008**, *112*, 1040.
[16] X. Hu, J. Schuster, S. E. Schulz, *J. Phys. Chem. C* **2017**, *121*, 28077.
[17] G. Kresse, J. Furthmüller, *Phys. Rev. B* **1996**, *54*, 1169.
[18] G. Kresse, J. Furthmüller, *Comput. Mater. Sci.* **1996**, *6*, 15.
[19] D. Joubert, *Phys. Rev. B* **1999**, *59*, 1758.
[20] P. E. Blöchl, *Phys. Rev. B* **1994**, *15*, 17953.
[21] S. Grimme, J. Antony, S. Ehrlich, H. Krieg, *J. Chem. Phys.* **2010**, *132*, 154104.
[22] S. Grimme, S. Ehrlich, L. Goerigk, *J. Comput. Chem.* **2011**, *32*, 1456.
[23] F. Zhou, M. Cococcioni, C. A. Marianetti, D. Morgan, G. Ceder, *Phys. Rev. B* **2004**, *70*, 235121.
[24] M. Raju, P. Ganesh, P. R. C. Kent, A. C. T. Van Duin, *J. Chem. Theory Comput.* **2015**, *11*, 2156.
[25] R. K. Chouhan, P. Raghani, *J. Appl. Phys.* **2015**, *118*, 125101.
[26] K. Persson, Y. Hinuma, Y. S. Meng, A. Van Der Ven, G. Ceder, *Phys. Rev. B Condens. Matter Mater. Phys.* **2010**, *82*, 125416.
[27] W. Humphrey, A. Dalke, K. Schulten, *J. Mol. Graph.* **1996**, *14*, 33.
[28] M. Yu, D. R. Trinkle, *J. Chem. Phys.* **2011**, *134*, 06411.
[29] R. S. Mulliken, *J. Chem. Phys.* **1955**, *23*, 1833.
[30] A. E. Reed, R. B. Weinstock, F. Weinhold, *J. Chem. Phys.* **1985**, *83*, 735.
[31] R. Dronskowski, P. E. Bloechl, *J. Phys. Chem.* **1993**, *97*, 8617.
[32] S. Maintz, V. L. Deringer, A. L. Tchougréeff, R. Dronskowski, *J. Comput. Chem.* **2016**, *59*, 24300.
[33] A. D. Bochevarov, E. Harder, T. F. Hughes, J. R. Greenwood, D. A. Braden, D. M. Philipp, D. Rinaldo, M. D. Halls, J. Zhang, R. A. Friesner, *Int. J. Quantum Chem.* **2013**, *113*, 2110.
[34] A. C. T. Van Duin, S. Dasgupta, F. Lorant, W. A. Goddard, *J. Phys. Chem. A* **2001**, *105*, 9396.
[35] G. Te Velde, F. M. Bickelhaupt, E. J. Baerends, C. Fonseca Guerra, S. J. A. van Gisbergen, J. G. Snijders, T. Ziegler, *J. Comput. Chem.* **2001**, *22*, 931.